COUPLING DISCRETE ELEMENT MODELS OF CERAMIC BREEDER PEBBLE BEDS TO THERMOFLUID MODELS OF HELIUM PURGE GAS USING VOLUME-AVERAGED NAVIER-STOKES AND THE LATTICE-BOLTZMANN METHOD

Jon T. Van Lew,* Alice Ying, Mohamed Abdou
Mechanical and Aerospace Engineering, UCLA, Los Angeles, CA 90095, USA,
**jtvanlew@fusion.ucla.edu*

Pebble-scale models of the interactions inside packed beds are critical for determining alterations to thermophysical properties in the wake of changes to the packed bed due to cracking, sintering, or creep-deformation of the ceramic pebbles. Simultaneously, the helium purge gas flow through the pebble bed can change; while not specifically playing a role as coolant, it does have an impact on the thermal transport in the volumetrically heated bed. We present numerical tools that are capable of resolving pebble-scale interactions coupled to bed-scale thermofluid flow. The new computational techniques are used to show that maximum temperatures in pebble beds do not increase drastically in spite of the significant amount of cracking induced in our numerical model. Furthermore a complete flow field of helium moving through densely packed spheres is modeled with the lattice-Boltzmann method to reveal the strong effect of slow-moving helium gas on flattening temperature profiles in pebble beds with nuclear heating.

I. BACKGROUND AND MOTIVATION

The solid breeder in many current designs for ITER feature sub-module units of packed beds.[1] From the point of view of pebble bed thermomechanics, this has the advantage of producing units individually that can be tested and qualified to desired packing states (and therefore thermomechanics) during the design phase.

We aim to provide designers of packed beds with tools to understand how packing states may evolve from time-dependent phenomena (*e.g.* sintering, creep, pebble cracking, *etc.*). These phenomena may, for instance: decrease the effective thermal conductivity which will raise bed temperatures beyond initial predictions, produce isolated pebbles which will sinter and potentially decrease tritium release rates, or even form gaps between pebble beds and containing structures, thus leading to divergence from initial packing properties.

Modeling research on ceramic pebble beds should have as its main objective a thorough understanding of the evolution of pebble bed morphology and the impact on thermophysical properties; allowing for temperature control of breeder pebble beds over the entire lifetime of the blanket. To accomplish that goal, this current study is aimed at developing a methodology for coupling established discrete element models of individual pebbles in the ensemble with thermo-fluid simulations of the interstitial helium purge gas. Specifically, we will address the impact of helium on the thermal transport in a bed with evolving morphology due to pebble cracking.

Global models of pebble beds and helium flow with pebble-scale detail are intractable with current computational hardware and modeling techniques. To overcome deficiencies in computational power, we introduce two new modeling approaches described in the following section that allow us to resolve pebble-scale interactions with bed-scale conjugate heat transfer with flowing gas.

II. NUMERICAL METHODOLOGY

Models based on the discrete element method (DEM) are currently the only tools available that can extract information on individual pebble interactions. The DEM formulation provides information such as inter-particle forces and individual particle temperatures, which are necessary for predicting and simulating morphological changes in the bed (*e.g.* pebble cracking, sintering, *etc*.) However DEM alone is not able to capture the effects, neither on momentum nor energy, of an interstitial fluid. Therefore we present two fluid modeling techniques to supplement the DEM computations. We will first discuss the fully dynamic coupling of the DEM model with a volume-averaged thermofluid model of helium. Then we will introduce the integration of our DEM packing structure into lattice-Boltzmann simulations of the entire bed-fluid system.

II.A. DEM Particles

In the DEM framework we track all the particles in the pebble bed in a Lagrangian manner. The position and rotation of every particle in the ensemble is explicitly integrated from balances of force and torque on individual pebbles. Introduced to the Newtonian force balance is a drag force term to capture interaction with surrounding fluid velocity fields. A thorough description of inter-particle contact physics in the standard DEM formulation is omitted here but can be found in excellent detail in

Refs. 2–4. The linear momentum and energy balances of particle, *i*, read:

$$m_i \frac{\mathrm{d}u_i}{\mathrm{d}t} = m_i g + \sum_{j=1}^{Z} F_{ij} + \beta_i V_i \Delta u_{if} \quad (1)$$

where m_i is the mass, g gravity, Z the coordination number of the particle, F_{ij} the inter-particle force, Δu_{if} is the relative velocity between the fluid and pebble, *i*, and the inter-phase momentum exchange coefficient, β_i, acts upon the pebble volume, V_i. And

$$m_i C_i \frac{\mathrm{d}T_i}{\mathrm{d}t} = Q_{\mathrm{n},i} + \sum_{j=1}^{Z} Q_{ij} + \beta_{E,i} A_i \Delta T_{if} \quad (2)$$

where the particle has thermal mass, $m_i C_i$, at temperature T_i, $Q_{\mathrm{n},i}$ is the nuclear heating rate of the particle. The particle conducts to a neighbor at a rate of Q_{ij}, the inter-phase energy exchange coefficient, $\beta_{E,i}$, acts upon the pebble surface area, A_i.

The trajectory of pebble *i* is updated based on the force terms on the right hand side of Eq. (1): gravity, contact forces between particles (or particle-wall), and a drag force. Similarly, the temperature of the particle updates with the terms from Eq. (2): nuclear heating rate, inter-particle conduction, and now a heat transfer with surrounding fluid.

Drag forces from fluid flows through packed beds are found from volume-averaged, empirical correlations of either numerical or experimental studies. Considering a small region of a packed bed surrounding our particle of interest, *i*, the non-dimensional drag force is found only as a function of the local packing fraction of that region. In the zero Reynolds number limit, the non-dimensional drag force reduces to a Stokes flow correlation that is only a function of the local packing fraction value, ϕ. For the value of particle Reynolds numbers seen by the helium purge gas, this is the dominant term. However, for a complete discussion of the non-dimensional drag terms see Refs. 5, 6. The correlation used in this study comes from the results of numerical studies of packed beds from Koch and Hill.[7]

For brevity, the complete correlation is omitted but an example of the inter-phase momentum transfer coefficient for low Reynolds flow, dense packing is given for a pebble of diameter, *d*, in a fluid with viscosity μ_f as:

$$\beta_i = \frac{180\mu_f}{d_i^2} \cdot \frac{\phi}{1-\phi} \quad (3)$$

The inter-phase energy transfer coefficient is of the same form as a traditional heat transfer coefficient and is calculated from the Nusselt number for the helium flow (with conductivity k_f) through a packed bed.

$$\beta_{E,i} = \frac{\mathrm{Nu}_i\, k_f}{d_i} \quad (4)$$

For the slow-moving purge of helium flow in ceramic packed beds of fusion reactors, it suffices to use the correlation, as a function of packing fraction, Reynolds and Prandtl numbers, given by Li and Mason, valid for $\mathrm{Re_p} < 200$ (Ref. 8).

$$\mathrm{Nu} = 2 + 0.6(1-\phi)^{3.5}\mathrm{Re}_p^{1/2}\mathrm{Pr}^{1/3} \quad (5)$$

Thus we have a formulation whereby a known fluid flow field and temperature throughout the domain, we can calculate the influence of that fluid on every particle's position and temperature. Next we will cover how we can calculate the flow field based on a volume-averaged influence of particles on the fluid.

II.B. Volume-averaged CFD Helium

The technique of coupling CFD to DEM was first proposed by Tsuji, et al.[9] In this formulation of the helium flow, a fluid cell is much larger than the individual particles (in application, this meant approx. 5~6 particles per cell) and as such, the particles themselves are not resolved in the fluid space but are simply introduced via volume-averaged terms. Therefore momentum and energy of a fluid flow through a solid phase is governed by volume-averaged Navier-Stokes and energy equations.[10] These equations are applied to a discretized volume of fluid space. For fluid cell, *k*, (Ref. 5)

$$\frac{\partial(\epsilon_k \rho_f)}{\partial t} + \nabla \cdot (\epsilon_k \rho_f u_f) = 0 \quad (6)$$

$$\frac{\partial(\epsilon_k u_f)}{\partial t} + \nabla \cdot (\epsilon_k u_f u_f) = -\frac{\epsilon_k}{\rho_f}\nabla p_f + \nabla \cdot (\nu_f \epsilon_k \nabla u_f) - \frac{S_k}{\rho_f} \quad (7)$$

$$\frac{\partial(\epsilon_k T_f)}{\partial \mathrm{t}} + \nabla \cdot (\epsilon_k u_f T_f) = \nabla \cdot (\alpha_\mathrm{f} \epsilon_k \nabla T_f) - \frac{E_k}{\rho_f C_f} \quad (8)$$

where the fluid void fraction is the complement of the solid packing fraction, $\epsilon = 1 - \phi$. The momentum and energy exchanges with the solid phase are represented in the source terms. They are volume-weighted sums of the drag forces and energy exchanges, respectively, for all particles in the discretized fluid cell:

$$S_k = \frac{1}{V_k}\sum_{\forall i \in k} \beta_i V_i \Delta u_{if} \quad (9)$$

$$E_\mathrm{k} = \frac{1}{V_\mathrm{k}}\sum_{\forall i \in \mathrm{k}} \beta_{E,i} A_i \Delta T_{if} \quad (10)$$

The inter-phase momentum and energy exchange coefficients act as the communicators between the particle information from the DEM solver and the fluid fields from CFD. Thus the motion and energy of the fluid field are intimately coupled with the particle positions and energy, but computational time is preserved by only considering volume-averaged values in the fluid domain. The cross-communication between fluid and solid is

accomplished with a coupling routine that is explained in detail in Refs. 11, 12.

II.C. Lattice Boltzmann Model

The volume-averaged approach of the CFD-DEM coupling is an effective and efficient method for solving transiently coupled helium flow and pebble interaction. However, there are cases when a complete knowledge of the tortuous flow of the interstitial helium is desired. But because the CFD-DEM solver does not resolve the pathways on the particle scale, knowledge of precise helium flow is not possible with that technique. Therefore we have also investigated a combination of DEM and LBM solvers.

The lattice-Boltzmann approach to fluid simulations is a growing field of numerical modeling and certainly this short study cannot do justice to a proper explanation of the underlying physics. Briefly, the LBM structure considers discrete density distribution functions on nodes in a lattice. These distributions can be thought of as 'density with a direction' pointing at neighboring nodes. Macroscopic properties of fluid density, velocity, and temperature can be deduced from the distribution functions. Refs. 13, 14 are textbooks with excellent discussion of the physics and applications of LBM theory to fluid dynamics problems.

The distribution function at a given node is explicitly updated in time in two steps: collision and streaming. The collision operator in the Boltzmann distribution is discretized and approximated by Bhatnagar, Gross, and Krook.[15] In the first step, collision rules dictate the distribution function at node, *l*, and the second step streams information to neighboring nodes. The discrete LBM equation that is equivalent to Navier-Stokes is:

$$\boldsymbol{f_l}(\boldsymbol{x}+\boldsymbol{e_l}\boldsymbol{\Delta t},\boldsymbol{t}+\boldsymbol{\Delta t})+\boldsymbol{f_l}(\boldsymbol{x},\boldsymbol{t})=\frac{\boldsymbol{1}}{\boldsymbol{\tau}}\left[\boldsymbol{f_l}(\boldsymbol{x},\boldsymbol{t})-\boldsymbol{f_l^{eq}}(\boldsymbol{x},\boldsymbol{t})\right] \quad (11)$$

where $\boldsymbol{e_l}$ are the unit vectors pointing in the discrete lattice directions. The relaxation time, $\boldsymbol{\tau}$, is a function of the lattice kinematic viscosity (and contains much of the physical information of the fluid). We have used the incompressible equilibrium distribution function, $\boldsymbol{f_l^{eq}}$, given by He and Luo to solve for density and velocity.[16] The collision operator for the thermal lattice is that given by Guo, et al.[17] The solver has two lattices overlaid upon each other. The first is used to solve for density and velocity. The second lattice uses the velocity at each node and solves for the passive temperature scalar. For our model we represented the pebbles with a resolution of 10 nodes per diameter. For the system analyzed, this resulted in two lattices that have nodal sizes of $\boldsymbol{201\times151\times501}$; requiring, in a total, about 30 million nodes to be updated at each time step.

In the DEM-LBM approach, DEM is used only to determine packing structure and contact forces. When the bed is settled, a snapshot of the structure is discretized and loaded into the LBM solver which then calculates temperature and velocity fields of both solid and fluid phases. There is no cross-communication in this technique as the packing structure is effectively frozen during the LBM calculations.

II.D. Numerical Solvers

II.D.1. CFD-DEM Coupling

The DEM particle tracking and position integration are realized with LAMMPS, a highly parallelizable, open-source Molecular Dynamics code by Sandia National Labs.[18] The granular contact and heat transfer models are packaged into LIGGGHTS, a modification of LAMMPS with powerful additions for granular material.[19, 20] The helium fluid domain is modeled with a modified PISO solver in the open-source numerical framework of OpenFOAM® from OpenCFD, Ltd (Ref. 21). The coupling between LIGGGHTS and OpenFOAM® is accomplished with open-source, modular C++ libraries maintained by the CFDEM Project.[12]

II.D.2. DEM and LBM Interaction

LIGGGHTS is used as a pure DEM solver (here, neglecting fluid interaction) to calculate the structure of the packed bed. In-house code discretizes the DEM volume into lattices with binary values distinguishing the lattice nodes as either a solid or fluid. The lattices, with appropriate collision operators on the nodes, were then implemented in the open-source, parallelized LBM toolkit, Palabos, maintained by FlowKit Ltd.[22]

III. MODELING SETUP AND PROCEDURE

The pebble bed has dimensions in the *x*-*y* directions of $20d\times15d$, respectively. There are structural walls at the x-limits of the domain. The walls provide cooling with a constant temperature boundary condition of 573 K. The domain is periodic in the *y*-limits. 10 000 pebbles were loaded into the system which went to a height of approximately $24d$ after the bed was vibration packed. The pebble bed had a roof loaded at the upper limit of the *z*-direction that was lowered by force-control up to 6 MPa. This bed is referred to as the 'well-packed' bed. This was meant to simulate a fresh, densely-packed bed that is under compressive load during fusion operation. As such, this would be when pebbles would be likely to crack during operation. Therefore, based on the well-packed bed, a second bed was generated by simulating crushed pebbles; crudely the extensive crushing is simulated by simply removing 10% of the pebbles at random from the ensemble and then allowing the bed to resettle, from the now-imbalanced gravity and inter-particle forces, to a new stable packing structure. This bed is then referred to

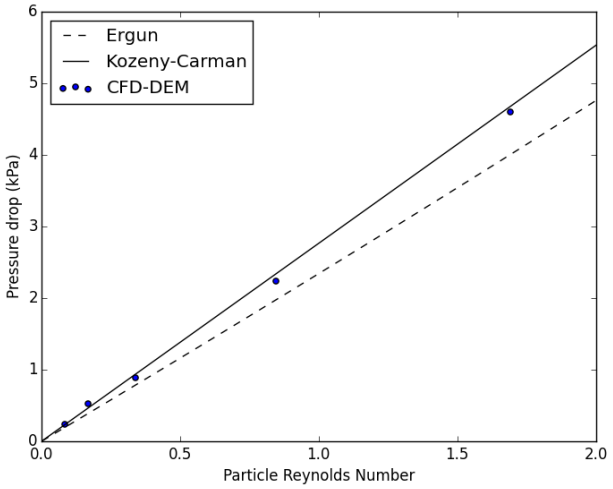

Fig. 1. Pressure drop from CFD-DEM model matches the Kozeny-Carman relation for the low particle Reynolds numbers appropriate for helium purge flow.

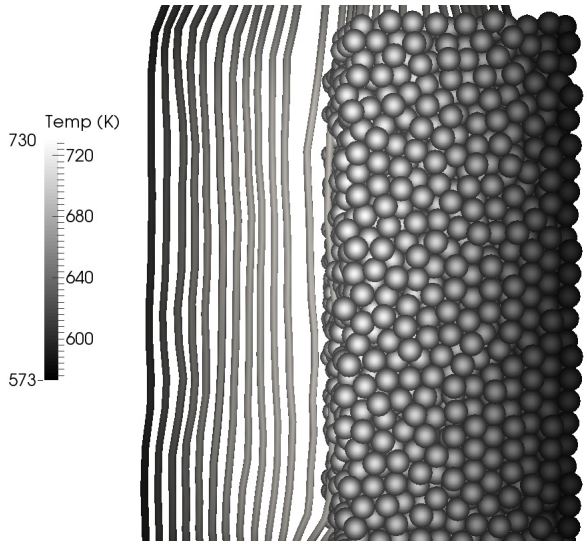

Fig. 2. View of the pebble bed with left-side cut away to show streamlines of helium moving in generally straight paths from inlet to exit.

as the 'resettled' bed for the rest of the analysis. The intent is to deduce changes in thermomechanical properties from an ideally packed bed to one where significant cracking has altered the ideal morphology of the bed.

The two pebble beds are analyzed in pure DEM, coupled CFD-DEM, and LBM simulations. The helium flow moves up the height of the bed from base to roof with a constant inlet velocity.

IV. RESULTS

Before analyzing thermal results from the CFD-DEM coupling, the system was run at various particle Reynolds numbers and the overall pressure drop of the packed bed was measured. This value was compared against the well-known Kozeny-Carman and Ergun equations. The Kozeny-Carman is known to fit better with experimental data at very small Reynolds numbers. In Fig. 1 we see the CFD-DEM coupling model is providing bed-scale pressure drops that match very well with Kozeny-Carman over the Reynold's numbers applicable to helium purge flow in fusion reactors.

The flow is visualized in Fig. 2. The pebble bed is clipped at the centerline to allow viewing of the helium streamlines. Apparent in the figure is temperature profiles in the helium from centerline to wall that qualitatively mirror temperature profiles in the pebble bed.

IV.A. Effective Thermal Conductivity of CFD-DEM

The well-packed and resettled pebble beds were run to thermal steady-state with nuclear heating and wall cooling in both pure DEM and coupled CFD-DEM simulations for comparison. From steady-state temperature distributions, seen in the pebble scatter plots in Fig. 3, an average profile is calculated and an effective thermal conductivity computed. The values are tabulated in Table I.

In the case of pure DEM, energy is transported solely along conduction routes in the ensemble. When the packing of the bed is disturbed, this results in a substantial drop in effective conductivity (a drop of 31%). The details of the conductivity reduction were studied extensively in Ref. 23. Perhaps more important than the reduction in effective conductivity, is the appearance of isolated pebbles. Because heat deposition is volumetrically applied, pebbles with poor conduction routes become much hotter than their neighbors. This is evident in the high temperatures seen in many of the pebbles in the right figure of Fig. 3. Over-heating of isolated pebbles could induce sintering and impact their tritium release even when the average temperatures measured in the bed are well below sintering values. There are two spikes in the average temperature plot of the pure DEM results. These arise from individual pebbles in the bottom of the ensemble which are completely isolated thermally from the rest of the pebble bed because of jammed 'bridges' of pebbles above them – they have no physical contact with any neighbors. The temperatures of those pebbles rise to artificially high values because of the adiabatic boundary of the bottom wall. In this case, there were two pebbles which are off the scale of the scatter plot, but their influence is seen in the average temperature of their region.

When CFD-DEM beds are analyzed, there is still a large reduction in effective conductivity (22% drop), but interesting to note is the lack of isolated pebbles with high temperatures. In the CFD-DEM scatter plot on the right

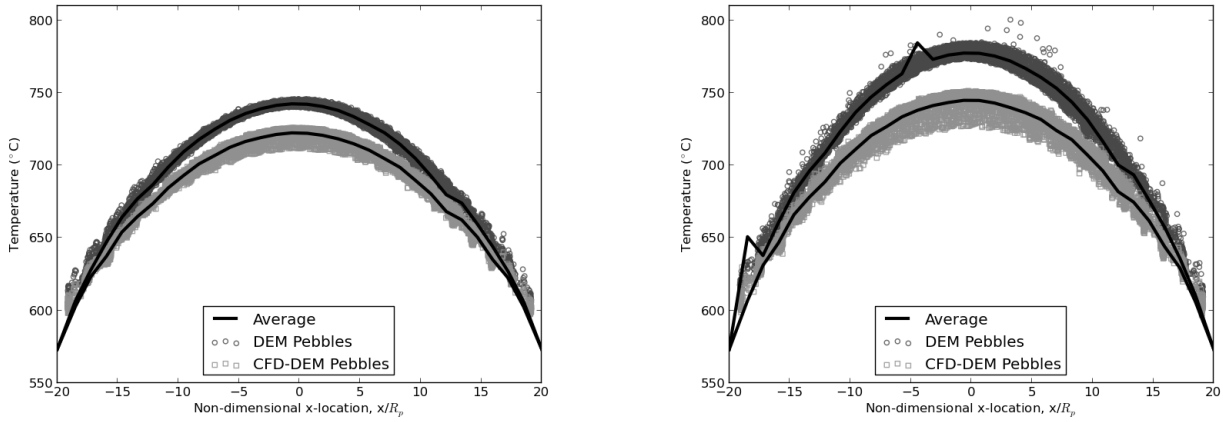

Fig. 3. Scatter temperature profiles of pebbles in a bed that is: well-packed (left) and resettled after 10% of pebbles were removed from crushing (right). The introduction of helium into the simulation contributes to both lower overall temperatures (higher effective conductivity) and the smoothing out of high temperatures of isolated pebbles.

image in Fig. 3, there is evidence of the reduced heat transfer in the same region as the isolated pebbles from the DEM bed, but the temperatures are much closer to the average values of neighboring pebbles. The helium purge gas has effectively smoothed out the temperatures and provided heat transport paths for any pebbles that have loose physical contact with neighbors.

In spite of the 22% decrease in effective conductivity, the maximum temperature of the pebble bed only increased 6.2% (from 725 to 751 K) when helium is included in the model. This result is significant for solid breeder designers. They may choose a solid breeder volume such that in the event of extensive pebble cracking, the maximum temperature of the bed would remain within the ideal windows dictate for the lithium ceramics.

TABLE I. Heat Transfer-Related Values from the Test Matrix of Pebble Beds.

	k_{eff} (W/mK)		$T_{\max}$ (K)		$\frac{Q_h}{Q_{nuc}}$ (%)
	DEM	CFDEM	DEM	CFDEM	CFDEM
Well-packed	0.96	1.09	745	725	1.15
Resettled	0.66	0.85	800	751	1.52

An accompanying result is the increased amount of energy carried out of the system by the helium purge gas. In Table I, the last column provides the ratio of energy carried out of the system to the nuclear energy deposited into the bed. The amount of energy carried out by the helium increased from 1.15% to 1.52% from 'well-packed' to 'resettled'.

IV.B. Laminar Mixing of Energy with LBM

In the CFD-DEM formulation, the slow-moving helium flow follows nearly straight, laminar streamlines from entrance to exit, as seen in Fig. 2. Therefore any contribution to thermal transport to the cooling structure would come only from conduction perpendicular to the flow. Thus we must resolve the fluid flow on the scale of the particle, for which the LBM technique is particularly adept.

In Fig. 4 we have plotted a small section of an *x*-*y* planar slice near the cooling walls. The solid regions in the figure are the representation of the pebbles in the LBM lattice. The interstitial helium flow is mapped with the vectors indicating velocity components perpendicular to the bulk flow along the *z*-axis. Apparent is the inward movement of helium away from cold regions near the wall where it mixes with hot helium moving outward from the centerline.

The pebble bed temperature profiles extracted from DEM and CFD-DEM simulations all could be fit precisely to parabolic curves. For a material with constant nuclear heating rate and constant thermal conductivity, the temperature profile is the parabola defined by:

$$\boldsymbol{T(x) - T_w = \eta\left(1 - \frac{x^2}{L^2}\right)} \tag{12}$$

where $\boldsymbol{\eta}$ is a constant, $\boldsymbol{\eta = q_n''' L^2 / 2k_{\text{eff}}}$. The ability to be fit to parabolic curves allowed calculating an effective thermal conductivity for the beds in those simulations.

However, the laminar mixing of energy seen in the helium results of LBM is manifest in the distortion of temperature profiles across the pebble bed. Shown in Fig. 5 is a profile of temperatures from

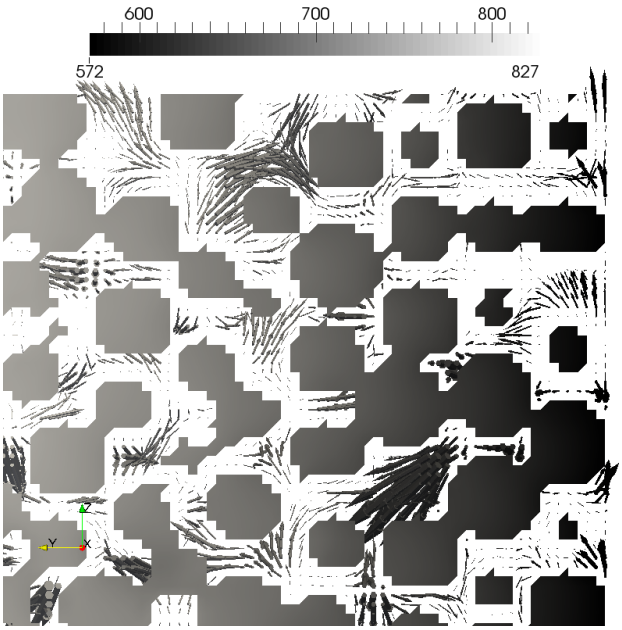

Fig. 4. A section of a slice in the x-y plane with projected velocity vectors of the fluid between solids. Showing helium flow perpendicular to the bulk movement along the *z*-axis – illustrating the laminar mixing of energy from helium flow.

a line located at a height of 10 pebble diameters from the inlet. Also shown on Fig. 5 are the bounding parabolas that are fit to match: (a) the slope at the wall to the LBM temperature profile, (b) the change in temperature from centerline to wall and (c) the integral value of temperature from the LBM result. The fit of (a) fits well near the wall but then greatly over-predicts the centerline temperature. The fit of (b) slightly under-predicts the temperature profile for the entire region of the pebble bed. The fit from (c) compares with the profile from LBM in a manner reminiscent of a turbulent velocity profile compared to a laminar velocity profile; that is the LBM curve has a sharper slope near the wall but is flatter near the centerline.

We note that the temperatures output in the lattice-Boltzmann model are much higher than those from the DEM or CFD-DEM simulations. This is attributed to the coarse resolution of pebbles on the lattice. Due to memory constrains, a resolution of 10 was the maximum that could be run. When >10 nodes/pebble diameter were used, the computer could not process the simulation. The low resolution resulted in poor contact between many pebbles and thus much poorer thermal transport to the cool boundaries and higher overall temperatures. We are in the process of repeating the LBM simulations with finer resolution running on upgraded hardware.

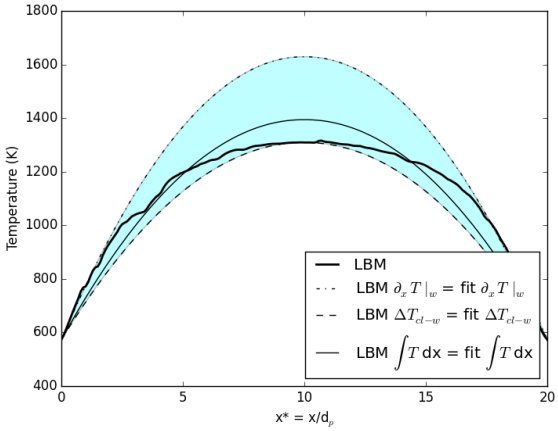

Fig. 5. Temperature profile from the LBM model is bound by parabolic curves. The LBM temperature profile increases sharply near the wall but then is flattened near the centerline. The behavior is indicative of laminar mixing of energy in the bed.

V. CONCLUSIONS

We have introduced two methods for effective modeling of a flowing interstitial helium gas interacting with a densely packed pebble bed under nuclear heating and wall cooling. The CFD-DEM formulation maintains calculations of pebble-pebble interactions while dynamically coupling to the helium flow. The model demonstrates the ability of helium gas to smooth out any hot spots predicted by pure-conduction DEM formulations. Further, the lattice-Boltzmann simulation, while not fully coupled to DEM, revealed important features of helium flow in volumetrically heated pebble beds – mainly the smearing of temperature profiles along the paths of cooling.

The findings presented in this paper are evidence of the usefulness of these computational tools for realizing pebble-scale thermomechanical interactions to further define pebble bed geometries allowing solid breeders to continue operating in an acceptable temperature window in spite of a large percentage of cracked pebbles. These tools can provide a mechanism for solid breeder engineers to design and qualify breeder modules to ensure proper operation throughout the blanket lifetime.

ACKNOWLEDGMENTS

This material is based upon work supported by the U.S. Department of Energy, Office of Science, Office of Fusion Energy Sciences, under Award Number DE-FG02-86ER52123.

REFERENCES

1. M. ZMITKO, Y. POITEVIN, L. BOCCACCINI, J. F. SALAVY, R. KNITTER, A. MÖSLANG, A. J. MAGIELSEN,

J. B. J. HEGEMAN, AND R. LÄSSER, "Development and qualification of functional materials for the EU Test Blanket Modules: Strategy and R&D activities," *J. Nucl. Mater.*, **417**, 678–683 (2011); http://dx.doi.org/10.1016/j.jnucmat.2011.02.009.

2. P. A. CUNDALL AND O. D. L. STRACK, "A discrete numerical model for granular assemblies," *Geotechnique*, **29**, 47–65 (1979); http://dx.doi.org/10.1680/geot.1979.29.1.47.
3. H. P. ZHU, Z. Y. ZHOU, R. Y. YANG, AND A. B. YU, "Discrete particle simulation of particulate systems: A review of major applications and findings," *Chem. Eng. Sci.*, **63**, 5728–5770 (2008); http://dx.doi.org/10.1016/j.ces.2008.08.006.
4. A. DI RENZO AND F. P. DI MAIO, "Comparison of contact-force models for the simulation of collisions in DEM-based granular flow codes," *Chem. Eng. Sci.*, **59**, 525–541 (2004); http://dx.doi.org/10.1016/j.ces.2003.09.037.
5. M. S. VAN BUIJTENEN, W.-J. VAN DIJK, N. G. DEEN, J. A. M. KUIPERS, T. LEADBEATER, AND D. J. PARKER, "Numerical and Experimental Study on Multiple-spout Fluidized Beds," *Chem. Eng. Sci.*, **66**, 2368–2376 (2011); http://dx.doi.org/10.1016/j.ces.2011.02.055.
6. M. A. VAN DER HOEF, R. BEETSTRA, AND J. A. M. KUIPERS, "Lattice-Boltzmann simulations of low-Reynolds-number flow past mono- and bidisperse arrays of spheres: results for the permeability and drag force," *J. Fluid Mech.*, **528**, 233–254 (2005); http://dx.doi.org/10.1017/S0022112004003295.
7. D. L. KOCH AND R. J. HILL, "Inertial Effects in Suspension and Porous-Media Flows," *Annu. Rev. Fluid Mech.*, **33**, 619–647 (2001); http://dx.doi.org/10.1146/annurev.fluid.33.1.619.
8. J. LI, D. J. MASON, AND A. S. MUJUMDAR, "A Numerical Study of Heat Transfer Mechanisms in Gas–Solids Flows Through Pipes Using a Coupled CFD and DEM Model," *Dry. Technol.*, **21**, 1839–1866 (2003); http://dx.doi.org/10.1081/DRT-120025511.
9. Y. TSUJI, T. TANAKA, AND T. ISHIDA, "Lagrangian numerical simulation of plug flow of cohesionless particles in a horizontal pipe," *Powder Technol.*, **71**, 239–250 (1992); http://dx.doi.org/10.1016/0032-5910(92)88030-L.
10. D. GIDASPOW, *Multiphase flow and fluidization: continuum and kinetic theory descriptions*. Academic press, (1994).
11. C. GONIVA, C. KLOSS, A. HAGER, AND S. PIRKER, "An Open Source CFD-DEM Perspective," *Proceedings of OpenFOAM Workshop, Göteborg*, 1–10 (2010).
12. C. GONIVA, C. KLOSS, N. G. DEEN, J. A. M. KUIPERS, AND S. PIRKER, "Influence of Rolling Friction on Single Spout Fluidized Bed Simulation," *Particuology*, **10**, 582–591 (2012); http://dx.doi.org/10.1016/j.partic.2012.05.002.
13. M. C. SUKOP AND D. T. THORNE, *Lattice Boltzmann Modeling - An Introduction for Geoscientists and Engineers*. Springer, (2006).
14. S. SUCCI, *The Lattice-Boltzmann Equation*. Oxford University Press, (2001).
15. P. BHATNAGAR, E. GROSS, AND M. KROOK, "A Model for Collision Processes in Gases. I. Small Amplitude Processes in Charged and Neutral One-Component Systems," *Phys. Rev.*, **94**, 511–525 (1954); http://dx.doi.org/10.1103/PhysRev.94.511.
16. X. HE AND L.-S. LUO, "Lattice Boltzmann Model for the Incompressible Navier–Stokes Equation," *J. Stat. Phys.*, **88**, 927–944 (1997); http://dx.doi.org/10.1023/B:JOSS.0000015179.12689.e4.
17. Z. GUO, B. SHI, AND C. ZHENG, "A coupled lattice BGK model for the Boussinesq equations," *Int. J. Numer. Methods Fluids*, **342**, 325–342 (2002); http://dx.doi.org/10.1002/fld.337.
18. S. PLIMPTON, "Fast Parallel Algorithms for Short-Range Molecular Dynamics," *J. Comput. Phys.*, **117**, 1–19 (1995); http://dx.doi.org/10.1006/jcph.1995.1039.
19. C. KLOSS AND C. GONIVA, "LIGGGHTS - Open Source Discrete Element Simulations of Granular Materials Based on LAMMPS," *Suppl. Proc. Mater. Fabr. Prop. Charact. Model.*, **2**, 781–788 (2011); http://dx.doi.org/10.1002/9781118062142.ch94.
20. C. KLOSS, C. GONIVA, A. HAGER, S. AMBERGER, AND S. PIRKER, "Models, algorithms and validation for opensource DEM and CFD-DEM," *Prog. Comput. Fluid Dyn.*, **12**, 140–152 (2012); http://dx.doi.org/10.1504/PCFD.2012.047457.
21. OPENCFD LTD., "OpenFOAM - The Open Source CFD Toolbox," 2.3.1, (2014).
22. FLOWKIT LTD., "Palabos." 1.5, (2014).
23. J. T. VAN LEW, A. YING, AND M. ABDOU, "A discrete element method study on the evolution of thermomechanics of a pebble bed experiencing pebble failure," *Fusion Eng. Des.*, **89**, 1151–1157 (2014); http://dx.doi.org/10.1016/j.fusengdes.2014.04.066.